MATHEMATICAL MODELING AND COMPUTING, Vol. 12, No. 1, pp. 116–131 (2025)

Chaotic dynamics of a new 7D memristor-based generator: computer modeling and circuit design

Kopp M. I.[1], Samuilik I.[2,3]

[1] *Institute for Single Crystals, NAS Ukraine, 60 Nauka Ave., Kharkiv 61072, Ukraine*
[2] *Institute of Life Sciences and Technologies, Daugavpils University, 13 Vienibas Str., LV-5401 Daugavpils, Latvia*
[3] *Institute of Applied Mathematics, Riga Technical University, LV-1048 Riga, Latvia*

(Received 8 July 2024; Accepted 26 September 2024)

The paper introduces a new seven-dimensional (7D) chaotic system based on a memristor emulator created using a hyperbolic tangent function. This system is derived from a six-dimensional (6D) dynamic system of equations that describes the process of magnetic field generation, serving as an alternative to the Rikitake dynamo, which explains the inversion of the magnetic field of the Earth and other celestial bodies. The study analyzes the stability of equilibrium points in the new dynamical system. The Lyapunov exponents spectrum and the Kaplan–Yorke dimension are calculated for fixed parameters of the 7D dynamical system. The presence of a positive Lyapunov exponent demonstrates the chaotic behavior of the new 7D dynamic system, while the fractional Kaplan–Yorke dimension indicates the fractal structure of strange attractors. Based on the results from Matlab–Simulink and LabVIEW models, a chaotic signal generator for the 7D chaotic memristive system is implemented in the Multisim environment. The chaotic behavior simulation in the Multisim environment exhibits similar results to the simulations in the Matlab–Simulink and LabVIEW models.

Keywords: *memristor-based dynamic systems; chaotic behavior; computer simulation; circuit implementation.*

2010 MSC: 76D05, 76D10, 76N20 **DOI:** 10.23939/mmc2025.01.116

1. Introduction

In recent years, there has been a significant increase in the study of chaotic systems due to their wide-ranging applications in physics, engineering, and related fields. Chaos refers to a deterministic yet unpredictable behavior that is characterized by a sensitive dependence on initial conditions. Nonlinear dynamic systems are known to exhibit chaotic behavior, making them a popular area of research. Chaotic systems with an attractor of dimensions above 3D have a wider practical application. It is preferred to use chaotic systems of a higher dimension for secure communication. The chaotic system has more complex dynamics in the presence of more than one Lyapunov exponent, which increases the security of information transmission. In addition, such systems are characterized by broadband, orthogonality, and complexity of the structure of chaotic signals, as well as strong sensitivity to initial conditions. These properties determine perspectives for their use for the secure transmission of information. Therefore, computer simulation of chaotic signals and the search for a circuit implementation of chaotic oscillation generators is an important problem [1–3].

It is known that many hyper-chaotic systems with unique features and properties have been discovered in recent years. One of the first hyper-chaotic systems is the Rössler system [4], and the circuit design was implemented by Matsumoto et al. [5]. The minimum dimension of a hyper-chaotic system with continuous time is four. Since the discovery of the first Rössler hyper-chaotic system, many 4D hyper-chaotic systems have been described in the literature, such as Lorentz's hyper-chaotic system [6], Liu's hyper-chaotic system [7], Chen's hyper-chaotic system [8], hyper-chaotic Wang system [9], hyper-chaotic Newton–Leipnik system [10], hyper-chaotic Vaidyanathan system [11–13]. A 5D hyper-chaotic Rikitake dynamo system with three positive Lyapunov exponents is proposed in papers [14, 15], that

has a hidden attractor without any equilibrium point. The paper [14] describes the modeling, circuitry, and engineering applications of a 5D hyper-chaotic dynamo.

Chaos generators based on memristors are a recent and rapidly emerging field in nonlinear circuit theory. Chua [16] originally used the term "memristor" to refer to a symmetrical principle-based device, where magnetic flux and electric charge are coupled. The concept of memristor systems has evolved over time to encompass a wider range of systems [17]. The HP laboratory achieved the first implementation of a metal–dielectric–metal memristor device [18]. A comprehensive review of memristive hyper-chaotic systems is provided in a monograph [19]. There are few examples in the literature of multidimensional hyper-chaotic systems based on memristors. Wang et al. [20] introduced a new 5D chaotic system with a flux-controlled memristor. Mezatio et al. [21] demonstrated a 6D autonomous system by integrating a flux-controlled memristor model into an existing 5D hyper-chaotic autonomous system. Kou et al. [22] introduced an unusual 7D complex chaotic system combined with a cubic memristor.

Our paper introduces a new seven-dimensional chaotic system based on a hyperbolic tangent type memristor, in contrast to the studies mentioned earlier. The proposed model is derived from a 6D chaotic dynamo system [23], that offers an alternative to the Rikitake equations describing the reversals of the Earth's magnetic field. The motivation for this paper stems from the wide application of deterministic chaos in various engineering problems, such as the development of telecommunications systems. Furthermore, the development of electronic circuits for new chaos generators that describe real physical phenomena enables the physical modeling of the equations of nonlinear dynamics as an alternative to numerical modeling. The objective of this paper is to construct computer models of a new seven-dimensional chaotic dynamic system using the Matlab–Simulink and LabVIEW software environments. For the circuit implementation of the new chaos generator, we utilize the Multisim package, to illustrate chaotic dynamics through phase portraits of attractors.

2. The development of a novel 7D memristor-based dynamic system

In this section, we present a new memristor chaotic system that combines a flux-controlled memristor with a 6D hyper-chaotic system. This system models the generation of a magnetic field through thermomagnetic effects in a non-uniformly rotating layer of an electrically conductive fluid under the influence of a constant vertical magnetic field $\mathbf{B}_0$. It is described by the following equations [23]:

$$\begin{cases} \dot{x}_1 = -x_1 + \mathrm{R}\, x_2 - 2x_4 - 0.1x_5, \\ \dot{x}_2 = \frac{1}{10}\left(-x_2 + x_1 - x_1x_3 - 0.002x_6 - 0.002x_6x_3\right), \\ \dot{x}_3 = \frac{1}{10}\left(-\frac{8}{3}x_3 + x_1x_2 + 0.002x_6x_2\right), \\ \dot{x}_4 = -x_4 + \frac{1}{10}x_1, \\ \dot{x}_5 = -x_5 + 32.87(1 + \mathrm{Ro})x_1 + 2x_6, \\ \dot{x}_6 = -x_6 - 0.01\mathrm{R}x_2 + 32.87x_4\mathrm{Ro} - \frac{1}{10}x_5. \end{cases} \tag{1}$$

In this system, the amplitudes of velocity field disturbances are denoted by x_1 and x_5, and magnetic field disturbances are represented by x_4 and x_6. Temperature field disturbances are expressed through the amplitudes x_2 and x_3. The parameter R, known as the Rayleigh number, acts as a bifurcation parameter. By adjusting its values, we can investigate a one-parameter array of solutions. The physical interpretation of R is associated with the temperature difference at the boundaries of the electrically conductive fluid layer. The Rossby parameter Ro characterizes the non-uniform rotation.

Let us consider a memristor model utilizing a hyperbolic tangent function. The mathematical expression for the memristor is:

$$\begin{cases} i_m = W(\varphi)\, u_m, \\ \frac{d\varphi}{dt} = u_m - k\,\varphi, \\ W(\varphi) = \tanh\varphi, \end{cases} \tag{2}$$

where i_m signifies the current flowing through the memristor, u_m denotes the voltage across the memristor, φ is the internal flux, $W(\varphi)$ represents the memductance, k is a positive parameter. The system

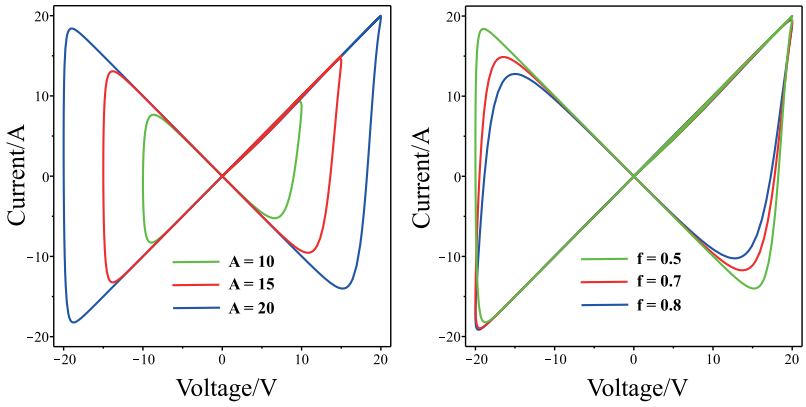

a ***b***

Fig. 1. Simulation of the hysteresis loop of a hyperbolic tangent type memristor for: (***a***) different amplitude values A; (***b***) different values of frequency f at $k = 1$.

of equations (2) generates nonlinear characteristic curves that pass through the origin. Using Maple software for numerical modeling of the system of equations (2), we assume the application of a sinusoidal alternating voltage $U = A\sin(2\pi ft)$ to the memristor input, where A and f represent the amplitude and external signal frequency, respectively. Figure 1 illustrates the results of modeling a memristor system (2). In case, when the memristor is excited by sinusoidal alternating current, its current-voltage characteristic forms a closed curve called a "hysteresis loop", passing through the origin. As the amplitude A increases, the area of the hysteresis loop expands, while an increase in frequency f causes it to gradually decrease. This behavior is typical of memristors.

As a result of combining equations (2) and (1), the equations for a seven-dimensional (7D) nonlinear dynamics are derived in the following form:

$$\begin{cases} \dot{x}_1 = -x_1 + \mathrm{R}\,x_2 - 2x_4 - 0.1x_5, \\ \dot{x}_2 = \frac{1}{10}\left(-x_2 + x_1 - x_1x_3 - 0.002x_6 - 0.002x_6x_3\right) - m\,W(x_7)\,x_1, \\ \dot{x}_3 = \frac{1}{10}\left(-\frac{8}{3}x_3 + x_1x_2 + 0.002x_6x_2\right), \\ \dot{x}_4 = -x_4 + \frac{1}{10}x_1, \\ \dot{x}_5 = -x_5 + 32.87(1 + \mathrm{Ro})x_1 + 2x_6, \\ \dot{x}_6 = -x_6 - 0.01\mathrm{R}x_2 + 32.87x_4\mathrm{Ro} - \frac{1}{10}x_5, \\ \dot{x}_7 = x_1 - x_7, \end{cases} \tag{3}$$

where m is a memristor parameter.

New dynamical variable x_7 is introduced instead of denoting the flux as φ.

As can be seen from equation (3), the system contains two controlled or bifurcation parameters: R and m. Furthermore, we will analyze the system of equations (3) for the two most important values of the nonuniformly rotation profiles: Keplerian $\mathrm{Ro} = -3/4$ and Rayleigh $\mathrm{Ro} = -1$. Subsequent sections of this article are devoted to the dynamic analysis of the newly introduced system (3).

3. Analysis of the novel 7D memristor-based system

This section provides a comprehensive exploration of both qualitative and numerical analyses of the recently introduced nonlinear dynamic system of equations (3).

3.1. Bifurcation diagrams, Lyapunov exponents and Kaplan–Yorke dimension

Using Mathematica's built-in function NDSolve, we solved the system of equations (3) with the initial conditions $x_1(0) = x_2(0) = x_3(0) = x_4(0) = x_5(0) = x_6(0) = 1$, $x_7(0) = 0$. Bifurcation diagrams were generated for the components x_1, x_2, x_4, x_5, x_6, x_7 of the nonlinear dynamic system (3), including a memristor, by varying the parameter R within the range $\mathrm{R} \in [0, 500]$ for two rotation parameters: $\mathrm{Ro} = -3/4$ and $\mathrm{Ro} = -1$. The bifurcation diagrams for $\mathrm{Ro} = -3/4$ and $m = 0.21$ are shown in Figure 2. These diagrams illustrate the transition to periodic, quasi-periodic, and chaotic modes depending on the values of R. Additionally, Figure 2 reveals that at a fixed parameter value of $\mathrm{R} = 59$, chaotic behavior in system (3) occurs for $m > 0.1$.

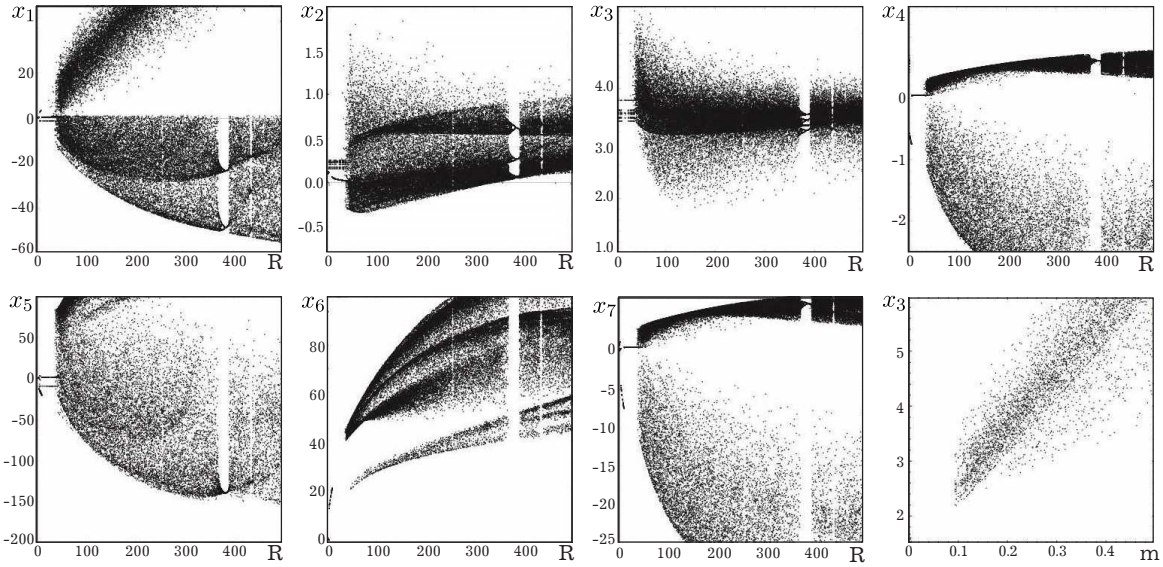

Fig. 2. Bifurcation diagrams for x_1, x_2, x_3, x_4, x_5, x_6, x_7 components of the system (3) at $\mathrm{Ro} = -3/4$ and $m = 0.21$ depending on changes in the parameter R; the bifurcation diagram for x_3 components of the system (3) at $\mathrm{Ro} = -3/4$ and $\mathrm{R} = 59$ depending on changes in the memristor parameter m.

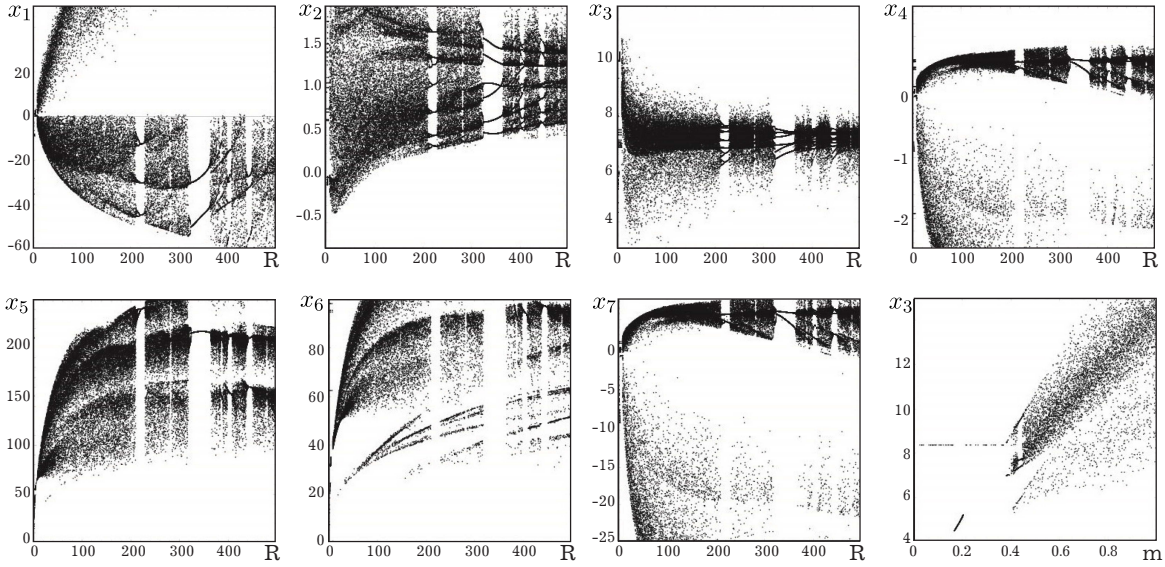

Fig. 3. Bifurcation diagrams for x_1, x_2, x_3, x_4, x_5, x_6, x_7 components of the system (3) at $\mathrm{Ro} = -1$ and $m = 0.5$ depending on changes in the parameter R; the bifurcation diagram for x_3 components of the system (3) at $\mathrm{Ro} = -1$ and $\mathrm{R} = 9$ depending on changes in the memristor parameter m.

Similarly, bifurcation diagrams were constructed for $\mathrm{Ro} = -1$ and $m = 0.5$ over the interval $\mathrm{R} \in [0, 500]$, as shown in Figure 3. As depicted in Figure 3, the system (3) exhibits chaotic behavior at a fixed parameter value of $\mathrm{R} = 9$, when $m > 0.4$.

The spectrum of Lyapunov exponents is a crucial element in defining the chaotic behavior of a nonlinear dynamical system. These exponents measure the rate of divergence or convergence of trajectories in phase space. Chaotic oscillations are indicated by the presence of at least one positive Lyapunov exponent. The dimension of the phase space of a nonlinear dynamical system corresponds to the number of Lyapunov exponents, and for our system (3), there are seven ones. Using the method described in [24,25], the maximum Lyapunov exponent for system (3) at $\mathrm{R} = 59$, $m = 0.21$, $\mathrm{Ro} = -3/4$ was calculated as $L_{\max} = 0.205641$. Through Gram–Schmidt orthogonalization, the following values for all Lyapunov exponents were obtained:

$$L_1 = 0.136412, \quad L_2 = 0.0294988, \quad L_3 = -0.823713,$$
$$L_4 = -0.955412, \quad L_5 = -1.13115, \quad L_6 = -1.19535, \quad L_7 = -1.42696.$$

The system (3) exhibits chaotic behavior since the spectrum includes a positive L_1, and L_2 is approaching zero. Given that $L_1+L_2+L_3+L_4+L_5+L_6+L_7=-5.3666742<0$, this dynamic system is dissipative.

The Kaplan–Yorke dimension for the chaotic system (3) is calculated as

$$D_{KY}=2+\frac{L_1+L_2}{|L_3|}\approx 2.2014.$$

Thus, the Lyapunov dimension of the chaotic system (3) is fractional. The Lyapunov exponents diagram for this system is shown in Figure 4*a*.

Similarly, the maximum Lyapunov exponent for system (3) at $\mathrm{R}=9$, $m=0.5$, $\mathrm{Ro}=-1$ was calculated as $L_{\max}=0.115566$. The more precise values of all Lyapunov exponents are:

$$L_1=0.0312055,\quad L_2\approx 0,\quad L_3=-0.552811,$$
$$L_4=-0.896204,\quad L_5=-1.01919,\quad L_6=-1.07702,\quad L_7=-1.85109.$$

This indicates that the system (3) also behaves chaotically under these parameters. The system is dissipative, as $L_1+L_2+L_3+L_4+L_5+L_6+L_7=-5.366672<0$, and the Kaplan–Yorke dimension is

$$D_{KY}=2+\frac{L_1+L_2}{|L_3|}\approx 2.0564.$$

Figure 4*b* illustrates the dynamics of Lyapunov exponents for the chaotic system (3) with parameters $\mathrm{R}=9$, $m=0.5$, $\mathrm{Ro}=-1$. Thus, in this section, we have demonstrated that the incorporation of a memristor enables the new 7D system (3) to exhibit chaotic behavior even at small values of the control parameter R.

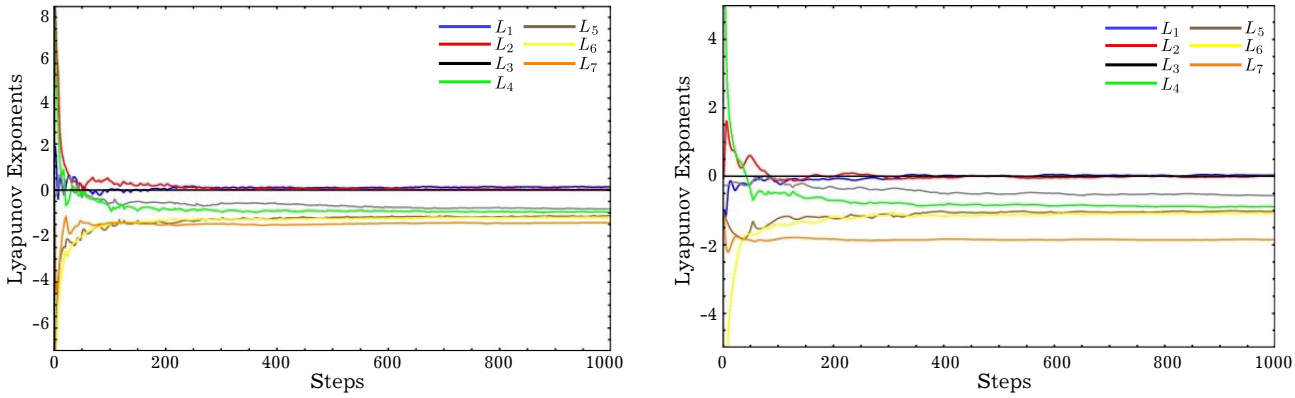

a ***b***

Fig. 4. The convergence plot of the Lyapunov spectrum for the system (3) at: (***a***) $\mathrm{R}=59$, $m=0.21$, $\mathrm{Ro}=-3/4$; (***b***) $\mathrm{R}=9$, $m=0.5$, $\mathrm{Ro}=-1$.

3.2. Basic properties

1. Symmetry. Unlike system (1), the coordinate transformation $\mathbf{T}(x_1,x_2,x_3,x_4,x_5,x_6,x_7)\to(-x_1,-x_2,x_3,-x_4,-x_5,-x_6,-x_7)$ in equations (3) is not satisfied due to the oddness of the hyperbolic tangent function. Therefore, the system (3) remains non-invariant under this transformation $\mathbf{T}$.

2. Dissipativity. The divergence of a vector field $\mathbf{\Phi}=(\dot{x}_1,\dot{x}_2,\dot{x}_3,\dot{x}_4,\dot{x}_5,\dot{x}_6,\dot{x}_7)$ is calculated as

$$\operatorname{div}\mathbf{\Phi}=\frac{\partial\dot{x}_1}{\partial x_1}+\frac{\partial\dot{x}_2}{\partial x_2}+\frac{\partial\dot{x}_3}{\partial x_3}+\frac{\partial\dot{x}_4}{\partial x_4}+\frac{\partial\dot{x}_5}{\partial x_5}+\frac{\partial\dot{x}_6}{\partial x_6}+\frac{\partial\dot{x}_7}{\partial x_7}=-5.367<0.$$

This indicates that the system (3) is dissipative, and it can give rise to chaotic attractors. Applying Liouville's theorem, we deduce that the phase volume exponentially diminishes to zero as time t approaches infinity: $V(t)=V(0)\exp(-5.367t)$.

3. Equilibrium points and stability. Setting the left-hand sides of equations (3) to zero for the case when $\mathrm{Ro}=-3/4$, one can get

$$\begin{cases} 0 = -\widetilde{x}_1 + \mathrm{R}\,\widetilde{x}_2 - 2\widetilde{x}_4 - 0.1\widetilde{x}_5, \\ 0 = \frac{1}{10}\left(-\widetilde{x}_2 + \widetilde{x}_1 - \widetilde{x}_1\widetilde{x}_3 - 0.002\widetilde{x}_6 - 0.002\widetilde{x}_6\widetilde{x}_3\right) - m\,W(\widetilde{x}_7)\,\widetilde{x}_1, \\ 0 = \frac{1}{10}\left(-\frac{8}{3}\widetilde{x}_3 + \widetilde{x}_1\widetilde{x}_2 + 0.002\widetilde{x}_6\widetilde{x}_2\right), \\ 0 = -\widetilde{x}_4 + \frac{1}{10}\widetilde{x}_1, \\ 0 = -\widetilde{x}_5 + 8.21\widetilde{x}_1 + 2\widetilde{x}_6, \\ 0 = -\widetilde{x}_6 - 0.01\mathrm{R}\,\widetilde{x}_2 - 24.65\widetilde{x}_4 - \frac{1}{10}\widetilde{x}_5, \\ 0 = \widetilde{x}_1 - \widetilde{x}_7 \end{cases}$$

for parameter values $\mathrm{R} = 59$ and $m = 0.21$, we obtained two equilibrium points denoted as

$$E_0(0,0,0,0,0,0,0), \quad E_1(-18.252, -0.455, 3.097, -1.825, -49.443, 50.206, -18.252). \tag{4}$$

Additionally, for parameter values $\mathrm{R} = 9$, $m = 0.5$, and $\mathrm{Ro} = -1$, we obtained also two equilibrium points denoted as

$$E_2(0,0,0,0,0,0,0), \quad E_3(-9.817, -1.604, 5.874, -0.981, -26.593, 27.003, -9.817). \tag{5}$$

When the system of equations (3) is linearized around the set of equilibria (4), the Jacobian matrix of the system is as follows:

$$J(E) = \begin{vmatrix} -1 & 59 & 0 & -2 & -0.1 & 0 & 0 \\ 0.1(1-\widetilde{x}_3) - 0.21\tanh\widetilde{x}_7 & -0.1 & -0.1(\widetilde{x}_1 + 0.002\widetilde{x}_6) & 0 & 0 & -0.0002(1+\widetilde{x}_3) & 0 \\ 0.1\widetilde{x}_2 & 0.1(\widetilde{x}_1 + 0.002\widetilde{x}_6) & -0.267 & 0 & 0 & 0.0002\widetilde{x}_2 & 0 \\ 0.1 & 0 & 0 & -1 & 0 & 0 & 0 \\ 8.21 & 0 & 0 & 0 & -1 & 2 & 0 \\ 0 & 0.59 & 0 & -24.65 & -0.1 & -1 & 0 \\ 1 & 0 & 0 & 0 & 0 & 0 & -1 \end{vmatrix}. \tag{6}$$

For Jacobian matrix (6), we find the characteristic polynomial $P(\lambda)$ and determine the eigenvalues for the equilibrium points. For point E_0,

$$\lambda_1 = -1, \quad \lambda_2 \approx 1.789, \quad \lambda_3 \approx -2.758, \quad \lambda_{4,5} \approx -1.163 \pm i\,0.630, \quad \lambda_6 \approx -0.804, \quad \lambda_7 \approx -0.267.$$

The equilibrium point E_0 is classified as a saddle point of index 1 because the Jacobian has one eigenvalue with a non-negative real part (an unstable eigenvalue). The eigenvalues for equilibrium point E_1 are

$$\lambda_1 = -1, \quad \lambda_{2,3} \approx 0.192 \pm i\,2.174, \quad \lambda_{4,5} \approx -1.214 \pm i\,0.959, \quad \lambda_6 \approx -1.733, \quad \lambda_7 \approx -0.588.$$

Because there are two unstable eigenvalues in the Jacobian matrix, the equilibrium point E_1 is classified as a saddle point of index 2.

In a similar way, we classify the equilibrium points $E_{2,3}$. Taking into account the values of parameters $\mathrm{R} = 9$ and $m = 0.5$ in the expression for the Jacobian matrix (6), for point E_2 we obtain the following eigenvalues:

$$\lambda_1 = -1, \quad \lambda_2 \approx 0.377, \quad \lambda_{3,4} \approx -1.108 \pm i\,1.078, \quad \lambda_5 \approx -0.611, \quad \lambda_6 \approx -1.648, \quad \lambda_7 \approx -0.267.$$

This shows that E_2 is an unstable saddle point of index 1.

The matrix $J = J(E_3)$ eigenvalues are found to be

$$\lambda_1 = -1, \quad \lambda_{2,3} \approx -0.00751 \pm i\,1.273, \quad \lambda_{4,5} \approx -1.066 \pm i\,1.022, \quad \lambda_6 \approx -1.637, \quad \lambda_7 \approx -0.581.$$

This demonstrates the stability of the equilibrium point E_3.

4. Computer modeling and electronic circuit design

This section employs computer modeling to investigate the dynamics of new 7D chaotic system. We utilize LabVIEW and Simulink, two visual design environments, to create chaotic oscillation generators for the 7D memristive system. Additionally, the circuit realization of the 7D memristor chaotic system has been successfully implemented within the Multisim environment.

4.1. Matlab–Simulink model

The equations (4) were numerically solved using a model developed in Matlab–Simulink. The Matlab–Simulink model of a chaotic oscillation generator consists of interconnected blocks for amplification, summation, subtraction, multiplication, integration, trigonometric functions, and signal recording. Gain blocks (Gain1–Gain14) contain information about the values of fixed parameters (3). The Con-

stant blocks hold data on the value of the Rayleigh parameter R and the memristor parameter m. Initially, we set the parameter values to R = 59 and $m = 0.21$ for the Keplerian rotation profile Ro $= -3/4$. Figure 5 illustrates the Matlab–Simulink model diagram. For the Rayleigh rotation pro-

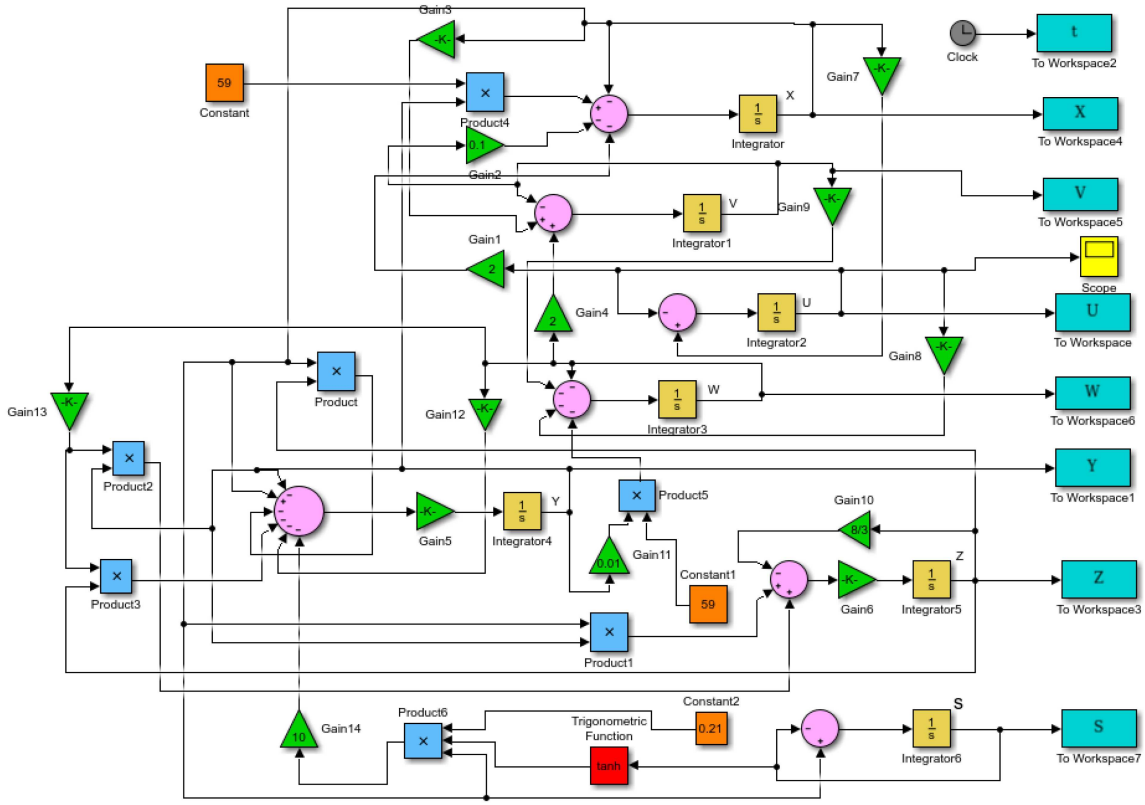

Fig. 5. The Matlab–Simulink model for equations (3) at fixed values of parameters: R = 59, $m = 0.21$, and Ro $= -3/4$. The simulation data is displayed using the To Workspace blocks.

file with fixed parameter values R = 9 and $m = 0.5$, adjustments must be made in the Matlab–Simulink diagram (see Figure 5), specifically changing the gain factors Gain3 from 8.21 → 0 and Gain8 from 24.65 → 32.87. The modeling results for the system of equations (3) with these parameters are shown in Figures 6 and 7. These figures reveal the complexity of the trajectories, characteristic of strange attractors. Note that directly implementing system 3) in an electronic circuit presents a certain challenge. The dynamic variables x_1, x_5, x_6, x_7 in (3) span a wide range of values, exceeding reasonable power supply limits. The operating voltage range of operational amplifiers in practical electronic circuits is typically −15 V to +15 V. This issue can be addressed by a simple transformation of the dynamic system's variables, as proposed in [26]. For our case, we need to rescale the following variables: $x_1 = 20X_1$, $x_5 = 50X_5$, $x_6 = 20X_6$, $x_7 = 2X_7$. The remaining variables are simply redesignated: $x_2 = X_2$, $x_3 = X_3$, $x_4 = X_4$. With this scaling, equations (3) are transformed

$$\begin{cases} \dot{X}_1 = -X_1 + 0.05\mathrm{R}X_2 - 0.1X_4 - 0.25X_5, \\ \dot{X}_2 = -0.1X_2 + 2X_1 - 2X_1X_3 - 0.004X_6 - 0.004X_3X_6 - 20m\tanh(2X_7)X_1, \\ \dot{X}_3 = -0.267X_3 + 2X_1X_2 + 0.004X_2X_6, \\ \dot{X}_4 = -X_4 + 2X_1, \\ \dot{X}_5 = -X_5 + 13.148(1 + \mathrm{Ro})X_1 + 0.8X_6, \\ \dot{X}_6 = -X_6 - 0.0005\mathrm{R}\,X_2 - 1.64\mathrm{Ro}\,X_4 - 0.25X_5, \\ \dot{X}_7 = 10X_1 - X_7. \end{cases} \tag{7}$$

Note that two systems (3) and (7) are equivalent since the linear transformation does not alter the physical properties of nonlinear systems. Next, in LabVIEW, we will obtain chaotic solutions of the equations (7) for the Keplerian rotation profile Ro $= -3/4$ and the Rayleigh rotation profile Ro $= -1$. These solutions will be compared with similar solutions obtained in Matlab–Simulink.

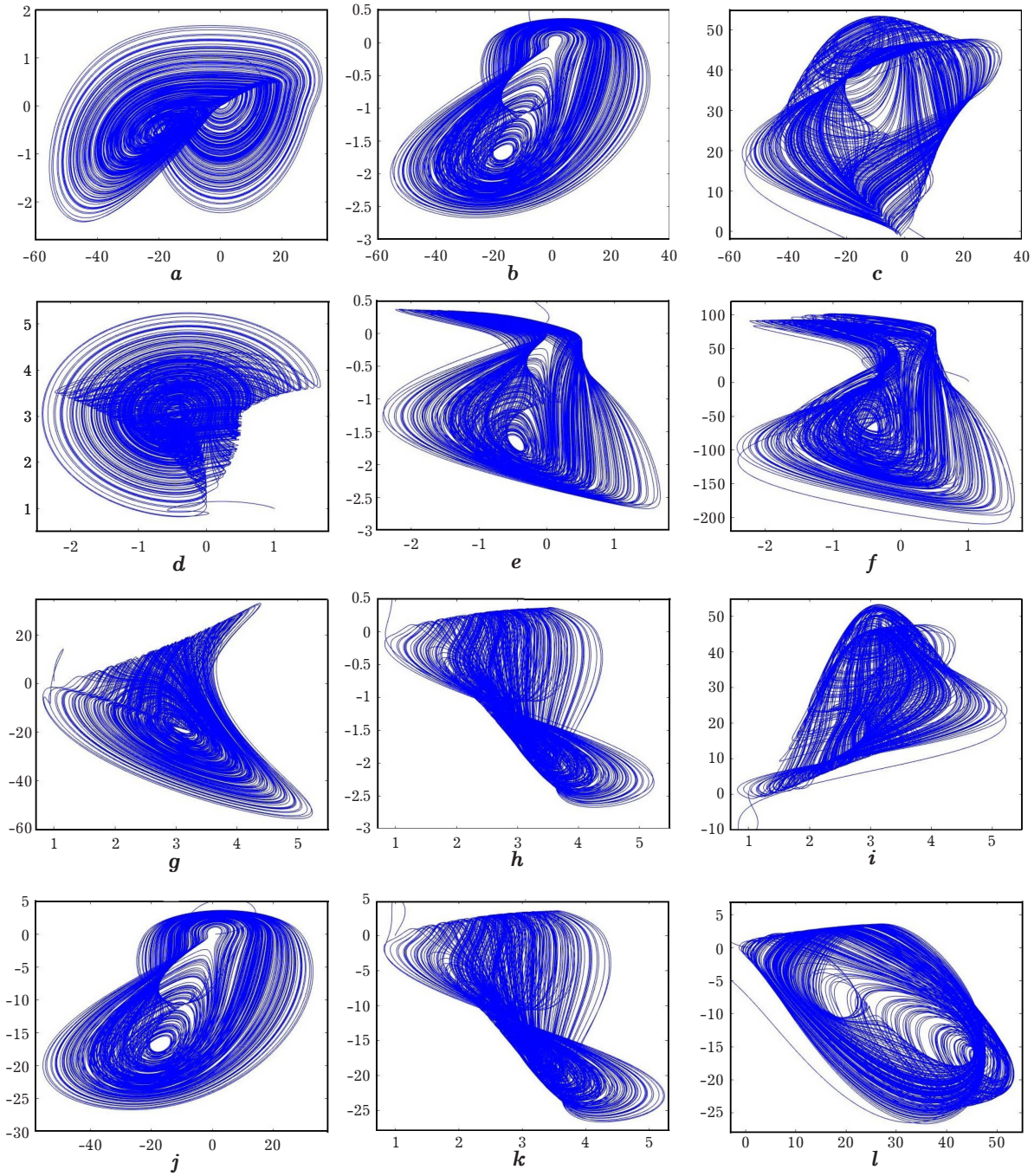

Fig. 6. Phase trajectories of the system (3) in different planes: (***a***) x_1x_2, (***b***) x_1x_4, (***c***) x_1x_6, (***d***) x_2x_3, (***e***) x_2x_4, (***f***) x_2x_5, (***g***) x_3x_1, (***h***) x_3x_4, (***i***) x_3x_6, (***j***) x_1x_7, (***k***) x_3x_7, (***l***) x_6x_7 at $\mathrm{Ro} = -3/4$, $\mathrm{R} = 59$ and $m = 0.21$.

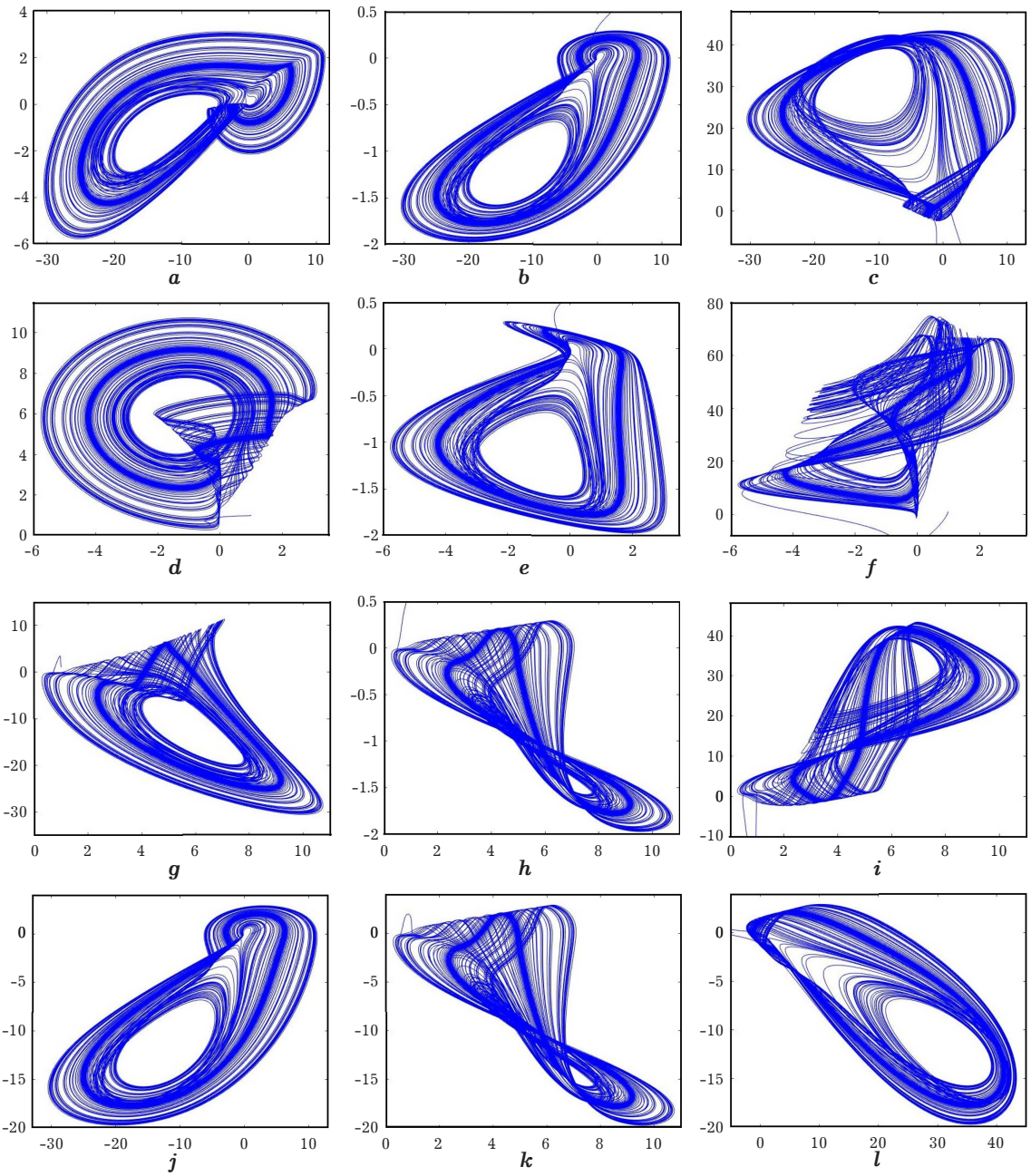

Fig. 7. Phase trajectories of the system (3) in different planes: (***a***) x_1x_2, (***b***) x_1x_4, (***c***) x_1x_6, (***d***) x_2x_3, (***e***) x_2x_4, (***f***) x_2x_5, (***g***) x_3x_1, (***h***) x_3x_4, (***i***) x_3x_6, (***j***) x_1x_7, (***k***) x_3x_7, (***l***) x_6x_7 at $\mathrm{Ro} = -1$, $\mathrm{R} = 9$ and $m = 0.5$.

4.2. LabVIEW model

The modeling of nonlinear dynamic systems using various software environments is of great interest as it allows for the demonstration of various informational properties of chaotic oscillations. To simulate the chaotic system (7) and showcase the results, we employ the LabVIEW software environment. LabVIEW is a graphical software platform widely used in engineering applications [27]. A visual platform has been created for the development of algorithms in LabVIEW.

Figure 8 depicts a block diagram of the chaotic system (7). This model was developed using the **Control & Simulation** and **Formula Node** toolkits, in contrast to earlier works [28, 29]. Equations (7) are expressed on their right-hand sides using the **Formula Node**. A more simplified block diagram is achieved by using a **Formula Node** instead of function blocks. **Integrator** blocks from the **Continuous** palette are utilized for time derivative integrations.

A LabVIEW model of chaotic solutions to the transformed equations (7) is presented in Figures 9 and 10 for both profiles: Ro $= -3/4$ and Ro $= -1$. The modeling results are displayed as phase portraits in planes such as X_2X_5, X_2X_4, X_3X_1, X_3X_4, X_1X_6, X_3X_6, X_1X_7, X_6X_7, X_1X_2 for initial conditions $X_1(0) = X_2(0) = X_3(0) = X_4(0) = X_5(0) = X_6(0) = 1$, $X_7 = 0$. Figures 9 and 10 illustrate how the reduced range of dynamic variable values enables the implementation of electronic circuits with operational amplifiers operating within a standard voltage range.

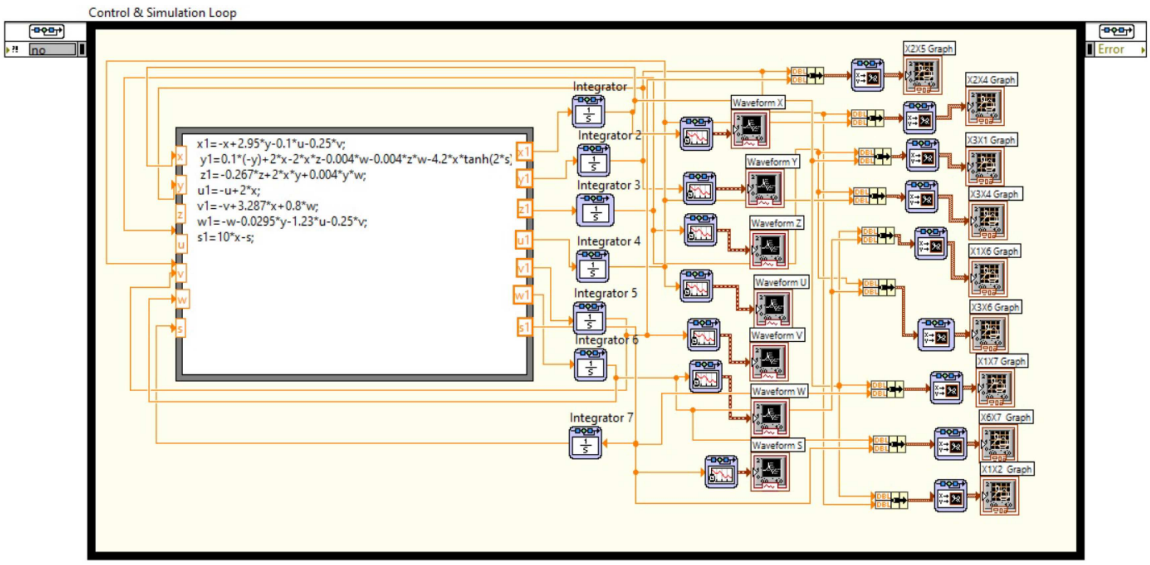

Fig. 8. The block diagram that implements the system (7) in LabVIEW.

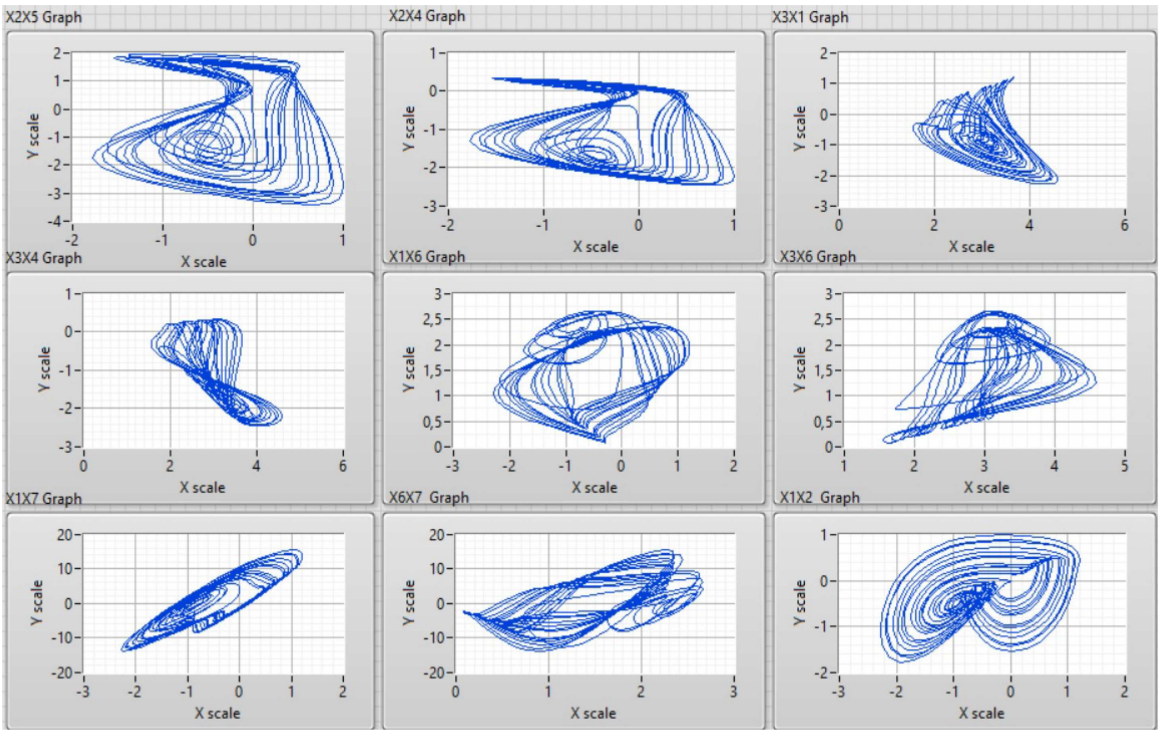

Fig. 9. Phase portraits of the rescaled system (7) at R $= 59$, $m = 0.21$, Ro $= -3/4$ in various planes obtained in LabVIEW.

4.3. Multisim modeling

An efficient method for exploring the dynamics of chaotic and hyper-chaotic systems is to use electronic circuits to simulate them. These circuits are essential for many chaos applications, including random bit generators, image encryption methods and other cutting-edge technologies.

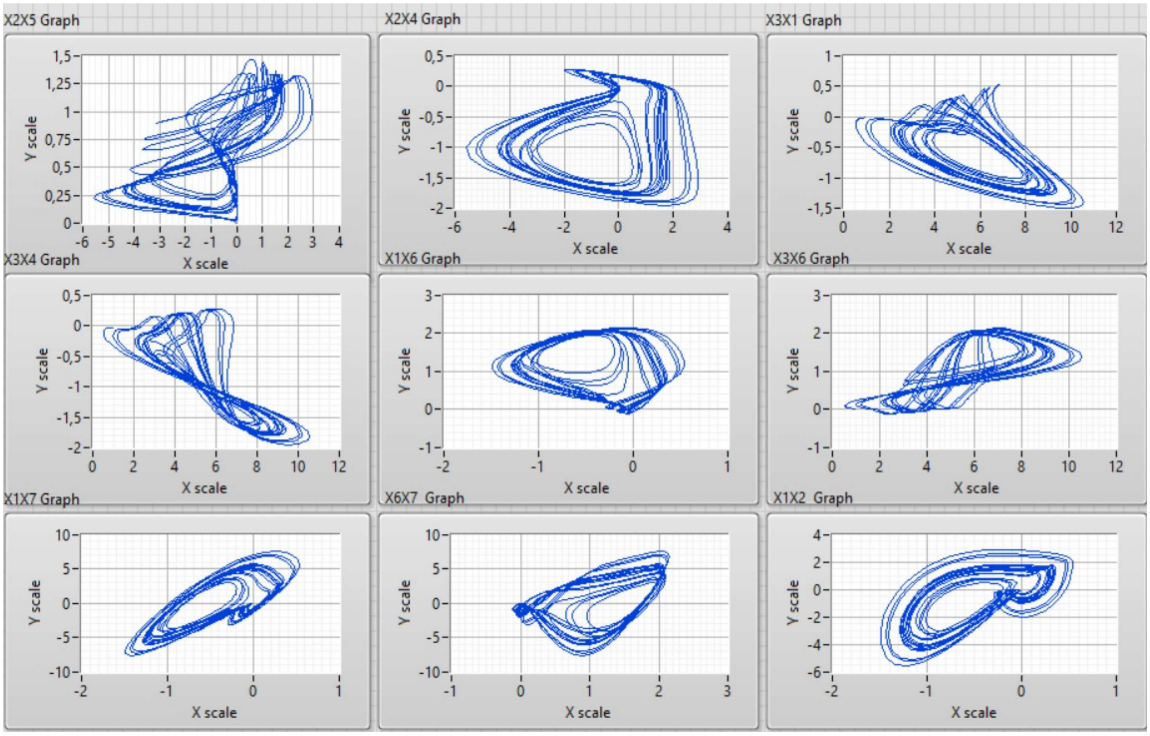

Fig. 10. Phase portraits of the rescaled system (7) at R = 9, $m = 0.5$, Ro $= -1$ in various planes obtained in LabVIEW.

In this subsection, we develop an analog circuit for the memristor chaotic system (7). The results obtained through Multisim simulation are then compared with the numerical results from Matlab–Simulink and LabVIEW. To translate the dynamic system of equations (7) into a circuit, seven operational amplifiers are used to perform the signal integration function. The variables of the dynamic system (7) are represented by electrical signals corresponding to the instantaneous voltage values on capacitors C_1, C_2, C_3, C_4, C_5, C_6, C_7, denoted as $U_1(\tau)$, $U_2(\tau)$, $U_3(\tau)$, $U_4(\tau)$, $U_5(\tau)$, $U_6(\tau)$, $U_7(\tau)$. In accordance with Kirchhoff's laws for electrical circuits, electrical analog of the system (7) takes the following form:

$$\begin{cases} C_1\dfrac{dU_1}{d\tau} = -\dfrac{U_1}{R_{11}} + \dfrac{U_2}{R_{12}} - \dfrac{U_4}{R_{13}} - \dfrac{U_5}{R_{14}}, \\ C_2\dfrac{dU_2}{d\tau} = -\dfrac{U_2}{R_{21}} + \dfrac{U_1}{R_{22}} - \dfrac{U_1U_3}{R_{23}K} - \dfrac{U_6}{R_{24}} - \dfrac{U_3U_6}{R_{25}K} - \dfrac{U_1\tanh(U_7)}{R_{26}K}, \\ C_3\dfrac{dU_3}{d\tau} = -\dfrac{U_3}{R_{31}} + \dfrac{U_1U_2}{R_{32}K} + \dfrac{U_2U_6}{R_{33}K}, \\ C_4\dfrac{dU_4}{d\tau} = -\dfrac{U_4}{R_{41}} + \dfrac{U_1}{R_{42}}, \\ C_5\dfrac{dU_5}{d\tau} = -\dfrac{U_5}{R_{51}} + \dfrac{U_1}{R_{52}} + \dfrac{U_6}{R_{53}}, \\ C_6\dfrac{dU_6}{d\tau} = -\dfrac{U_6}{R_{61}} - \dfrac{U_2}{R_{62}} - \dfrac{U_4}{R_{63}} - \dfrac{U_5}{R_{64}}, \\ C_7\dfrac{dU_7}{d\tau} = -\dfrac{U_7}{R_{71}} + \dfrac{U_1}{R_{72}}, \end{cases} \tag{8}$$

where R_{ij} are resistors $(i, j) = 1, 2, 3, 4, 5, 6, 7$; K is a scaling coefficient for the multiplier. We choose the normalized resistor as $R_0 = 10\,\text{k}\Omega$ and the normalized capacitor as $C_0 = 100\,\text{nF}$. Then the time constant is equal to $t_0 = R_0C_0 = 10^{-3}\,\text{s}$. We rescale the state variables of the system (8) as follows $U_1 = U_0\widetilde{X}_1$, $U_2 = U_0\widetilde{X}_2$, $U_3 = U_0\widetilde{X}_3$, $U_4 = U_0\widetilde{X}_4$, $U_5 = U_0\widetilde{X}_5$, $U_6 = U_0\widetilde{X}_6$, $K = U_0K^{'}$, and $\tau = t_0t$. Next, we can write equations (8) in a dimensionless form. By substituting R_0, $C_1 = C_2 = C_3 = C_4 = C_5 = C_6 = C_0$, and $K^{'} = 10$ into (8) and comparing numerical values before the output voltages of the

system (8) and (7) for parameter values R = 59, $m = 0.21$, Ro $= -3/4$, we get the value of electronic circuit resistors:

$$\begin{cases} \dfrac{d\widetilde{X}_1}{dt} = -\dfrac{10\text{k}}{10\text{k}}\widetilde{X}_1 + \dfrac{10\text{k}}{3.39\text{k}}\widetilde{X}_2 - \dfrac{10\text{k}}{100\text{k}}\widetilde{X}_4 - \dfrac{10\text{k}}{40\text{k}}\widetilde{X}_5, \\ \dfrac{d\widetilde{X}_2}{dt} = -\dfrac{10\text{k}}{100\text{k}}\widetilde{X}_2 + \dfrac{10\text{k}}{5\text{k}}\widetilde{X}_1 - \dfrac{10\text{k}}{500\cdot 10}\widetilde{X}_1\widetilde{X}_3 - \dfrac{10\text{k}}{2.5\text{M}}\widetilde{X}_6 - \dfrac{10\text{k}}{250\text{k}\cdot 10}\widetilde{X}_3\widetilde{X}_6 - \dfrac{10\text{k}}{238\cdot 10}\widetilde{X}_1\tanh(\widetilde{X}_7), \\ \dfrac{d\widetilde{X}_3}{dt} = -\dfrac{10\text{k}}{37.45\text{k}}\widetilde{X}_3 + \dfrac{10\text{k}}{500\cdot 10}\widetilde{X}_1\widetilde{X}_2 + \dfrac{10\text{k}}{250\text{k}\cdot 10}\widetilde{X}_2\widetilde{X}_6, \\ \dfrac{d\widetilde{X}_4}{dt} = -\dfrac{10\text{k}}{10\text{k}}\widetilde{X}_4 + \dfrac{10\text{k}}{5\text{k}}\widetilde{X}_1, \\ \dfrac{d\widetilde{X}_5}{dt} = -\dfrac{10\text{k}}{10\text{k}}\widetilde{X}_5 + \dfrac{10\text{k}}{3.042\text{k}}\widetilde{X}_1 + \dfrac{10\text{k}}{12.5\text{k}}\widetilde{X}_6, \\ \dfrac{d\widetilde{X}_6}{dt} = -\dfrac{10\text{k}}{10\text{k}}\widetilde{X}_6 - \dfrac{10\text{k}}{339\text{k}}\widetilde{X}_2 - \dfrac{10\text{k}}{8.13\text{k}}\widetilde{X}_4 - \dfrac{10\text{k}}{40\text{k}}\widetilde{X}_5, \\ \dfrac{d\widetilde{X}_7}{dt} = -\dfrac{10\text{k}}{10\text{k}}\widetilde{X}_7 + \dfrac{10\text{k}}{1\text{k}}\widetilde{X}_1. \end{cases} \tag{9}$$

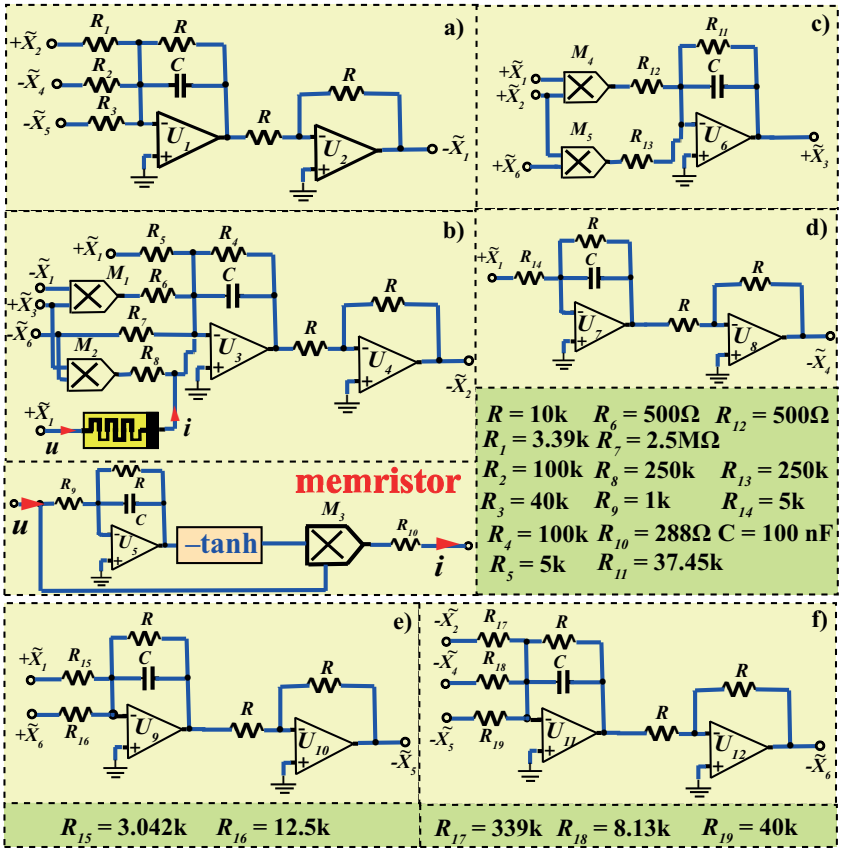

Fig. 11. Circuit modules for equation components (9): (*a*) $\widetilde{X}_1$, (*b*) $\widetilde{X}_2$, (*c*) $\widetilde{X}_3$, (*d*) $\widetilde{X}_4$, (*e*) $\widetilde{X}_5$, (*f*) $\widetilde{X}_6$ and the memristor circuit module, including an equation for $\widetilde{X}_7$ component.

Figure 11 illustrates analog circuit modules for the equations of system (9). The functionality of the chaos generator circuit diagram was tested in the Multisim environment. This circuit schematic is built using operational amplifiers TL084ACN and analog multipliers M_1, M_2, M_3, M_4, and M_5. Typically, AD633 series multipliers are utilized in practical applications.

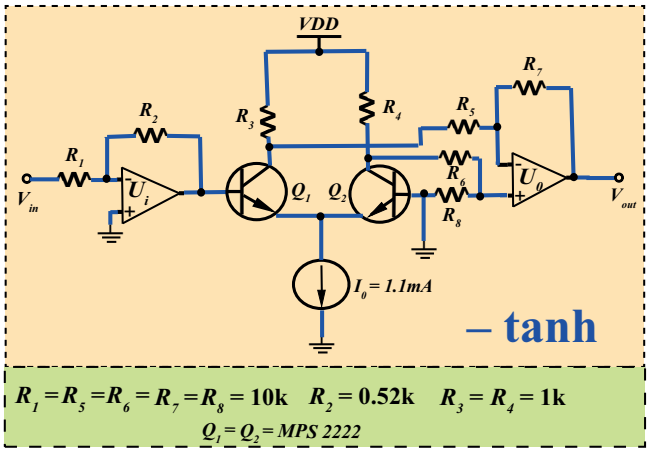

Fig. 12. Circuit scheme for realization of hyperbolic tangent function.

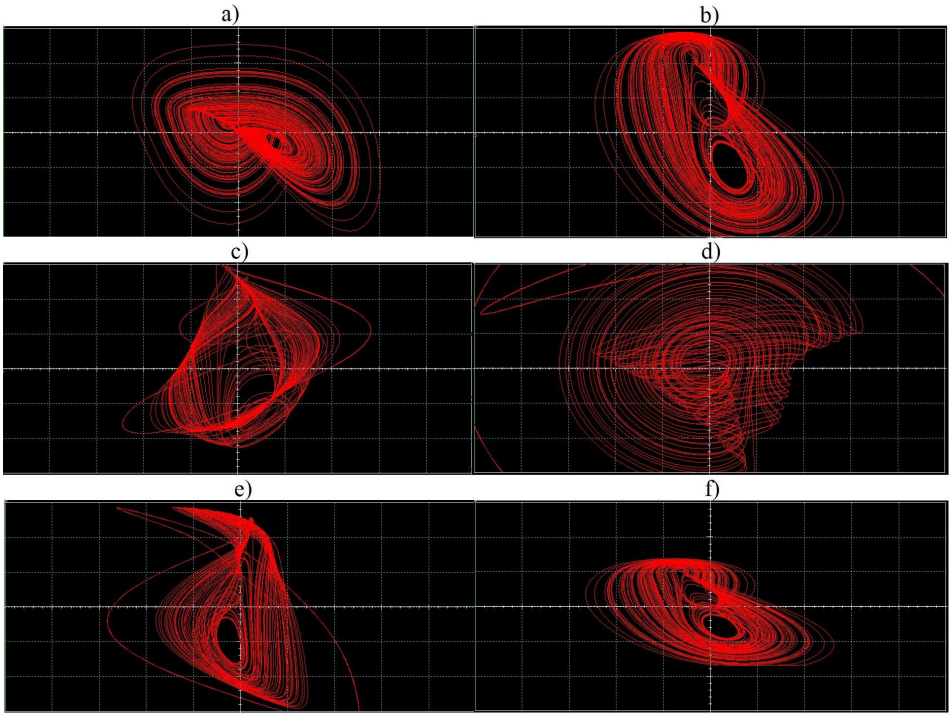

Fig. 13. Chaotic phase trajectories of a memristor electronic circuit (Figure 11) displayed in Multisim oscilloscopes: (***a***) $\widetilde{X}_1\widetilde{X}_2$ plane with scales 1 V/div and 1 V/div, (***b***) $\widetilde{X}_1\widetilde{X}_4$ plane with scales 1 V/div and 500 mV/div, (***c***) $\widetilde{X}_1\widetilde{X}_6$ plane with scales 1 V/div and 500 mV/div, (***d***) $\widetilde{X}_2\widetilde{X}_3$ plane with scales 500 mV/div and 500 mV/div, (***e***) $\widetilde{X}_2\widetilde{X}_4$ plane with scales 1 V/div and 500 mV/div, (***f***) $\widetilde{X}_1\widetilde{X}_7$ plane with scales 1 V/div and 5 V/div.

The electronic circuit for a memristor emulator based on the hyperbolic tangent function is frequently used in studies of the dynamics of memristive Hopfield neural networks (see, for example [30, 31]). As depicted in Figure 12, the equivalent circuit for the inverting hyperbolic tangent function comprises two transistors MPS2222 (Q1 and Q2), two operational amplifiers TL084ACN, one current source $I_0 = 1.1\,\text{mA}$, and numerous resistors. Operational amplifiers are responsible for subtraction and input inversion, while transistors are employed for realizing the exponential operation.

By connecting a dual-channel oscilloscope to different outputs, we obtain various phase portraits in the Multisim environment, as shown in Figure 13. The Multisim outputs in Figure 13 and the LabVIEW outputs in Figure 9 exhibit similar results. Based on the above, we derived the Kirchhoff equations according to equations (7) for parameter values R = 9, $m = 0.5$, Ro $= -1$. For this case, in the electronic circuits presented in Figure 11, the values of the following resistors need to be adjusted:

$$R_1 \to 2.222\,\text{k}, \quad R_{17} \to 222.2\,\text{k}, \quad R_9 \to 2\,\text{k}, \quad R_{10} \to 100\,\Omega.$$

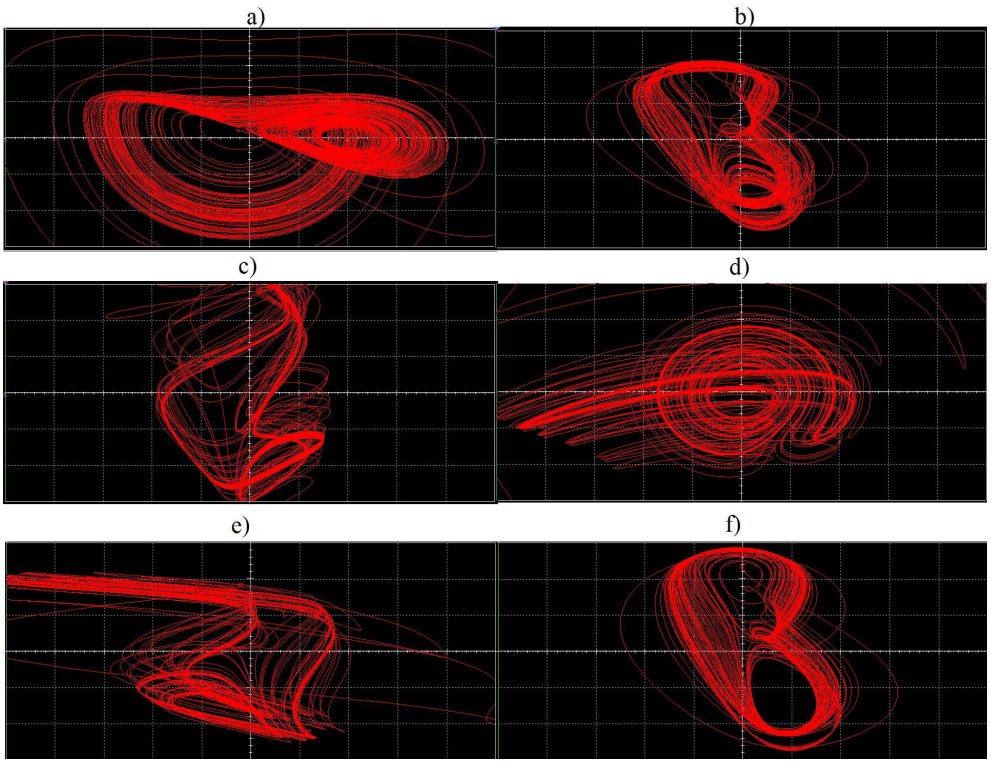

Fig. 14. Chaotic phase trajectories of a memristor modified electronic circuit (for the case $\mathrm{Ro} = -1$) displayed in Multisim oscilloscopes: (***a***) $\widetilde{X}_1\widetilde{X}_2$ plane with scales 1 V/div and 2 V/div, (***b***) $\widetilde{X}_1\widetilde{X}_4$ plane with scales 2 V/div and 1 V/div, (***c***) $\widetilde{X}_1\widetilde{X}_6$ plane with scales 2 V/div and 500 mV/div, (***d***) $\widetilde{X}_2\widetilde{X}_3$ plane with scales 1 V/div and 1 V/div, (***e***) $\widetilde{X}_2\widetilde{X}_4$ plane with scales 1 V/div and 1 V/div, (***f***) $\widetilde{X}_1\widetilde{X}_7$ plane with scales 2 V/div and 2 V/div.

The results of modeling modified electronic circuits of a chaos generator based on a memristor, accounting for the new resistor ratings, are presented in Figure 14. It is evident that the phase portraits of chaotic attractors closely resemble the LabVIEW simulation results shown in Figure 10.

5. Conclusion

In this paper, we propose a new 7D chaotic system based on a hyperbolic tangent-type memristor and explore its dynamics. We investigate fundamental properties of the system, such as Lyapunov exponents and the Kaplan–Yorke dimension, along with detailed descriptions of its phase portraits. We utilize Matlab–Simulink and LabVIEW models for numerical simulations of the nonlinear dynamic equations. Through phase portraits obtained from Matlab–Simulink and LabVIEW simulations, we observe that the oscillations in the systems exhibit complex, chaotic characteristics at defined values of the memristor parameter. Subsequently, an electronic circuit for a chaos generator tailored to the novel 7D dynamic system is designed. The performance of this electronic circuit in the Multisim environment is validated. Our work involves computing and modeling two chaotic generators derived from dynamic equations for Keplerian and Rayleigh rotation profiles. The integration of these generators with chaotic behavior into electronic devices holds promise for the development of more secure communication systems.

[1] Radwan A. G., Fouda M. E. On the Mathematical Modeling of Memristor, Memcapacitor, and Meminductor. Springer Cham (2015).

[2] Azar A. T., Vaidyanathan S., Ouannas A. Fractional Order Control and Synchronization of Chaotic Systems. Springer Cham (2017).

[3] Boubaker O., Jafari S. Recent advances in Chaotic systems and synchronization: from theory to real world applications. London, Academic Press (2019).

[4] Rössler O. E. An equation for hyperchaos. Physics Letters A. **71** (2–3), 155–157 (1979).

[5] Matsumoto T., Chua L., Kobayashi K. Hyperchaos: laboratory experiment and numerical confirmation. IEEE Transactions on Circuits and Systems. **33** (11), 1143–1147 (1986).

[6] Jia Q. Hyperchaos generated from the Lorenz chaotic system and its control. Physics Letters A. **366** (3), 217–222 (2007).

[7] Chen A., Lu J., Lu J., Yu S. Generating hyperchaotic Lü attractor via state feedback control. Physica A. **364**, 103–110 (2006).

[8] Li X. Modified projective synchronization of a new hyperchaotic system via nonlinear control. Communications in Theoretical Physics. **52** (2), 274–278 (2009).

[9] Wang J., Chen Z., Chen G., Yuan Z. A novel hyperchaotic system and its complex dynamics. International Journal of Bifurcation and Chaos. **18** (11), 3309–3324 (2008).

[10] Ghosh D., Bhattacharya S. Projective synchronization of new hyperchaotic system with fully unknown parameters. Nonlinear Dynamics. **61**, 11–21 (2010).

[11] Vaidyanathan S. A ten-term novel 4D hyperchaotic system with three quadratic nonlinearities and its control. International Journal of Control Theory and Applications. **6** (2), 97–109 (2013).

[12] Vaidyanathan S. Qualitative Analysis and Properties of a Novel 4-D Hyperchaotic System with Two Quadratic Nonlinearities and Its Adaptive Control. Advances in Chaos Theory and Intelligent Control. 455–480 (2016).

[13] Vaidyanathan S., Volos Ch. K., Pham V. T. Hyperchaos, adaptive control and synchronization of a novel 5-D hyperchaotic system with three positive Lyapunov exponents and its SPICE implementation. Archives of Control Sciences. **24** (4), 409–446 (2014).

[14] Vaidyanathan S., Pham V.-T., Volos C. K. A 5D hyperchaotic Rikitake dynamo system with hidden attractors. The European Physical Journal Special Topics. **224**, 1575–1592 (2015).

[15] Vaidyanathan S., Sambas A., Abd-El-Atty B., El-Latif A. A. A., Tlelo-Cuautle E., Guillén-Fernández O., Mamat M., Mohamed M. A., Alçin M., Tuna M., Pehlivan İ., Koyuncu İ., Ibrahim M. A. H. A 5D Multi-Stable Hyperchaotic Two-Disk Dynamo System With No Equilibrium Point: Circuit Design, FPGA Realization and Applications to TRNGs and Image Encryption. IEEE Access. **9**, 81352–81369 (2021).

[16] Chua L. O. Memristor-the missing circuit element. IEEE Transactions on Circuit Theory. **18** (5), 507–519 (1971).

[17] Chua L. O., Kang S. M. Memristive Devices and Systems. Proceedings of the IEEE. **64** (2), 209–223 (1976).

[18] Strukov D. B., Snider G. S., Stewart D. R., Williams R. S. The missing memristor found. Nature. **453**, 80–83 (2008).

[19] Sundarapandian V., Volos Ch. Advances in Memristors, Memristive Devices and Systems. Springer Cham, Switzerland (2017).

[20] Wang R., Li M., Gao Z., Sun H. A New Memristor-Based 5D Chaotic System and Circuit Implementation. Complexity. **2018**, 6069401 (2018).

[21] Mezatio B. A., Motchongom M. T., Tekam B. R. W., Kengne R., Tchitnga R., Fomethe A. A novel memristive 6D hyperchaotic autonomous system with hidden extreme multistability. Chaos, Solitons & Fractals. **120**, 100–115 (2019).

[22] Kou L., Huang Z., Jiang C., Zhang F., Ke W., Wan J., Liu H., Li H., Lu J. Data encryption based on 7D complex chaotic system with cubic memristor for smart grid. Frontiers in Energy Research. **10**, 980863 (2022).

[23] Kopp M. I., Tur A. V., Yanovsky V. V. Chaotic dynamics of magnetic fields generated by thermomagnetic instability in a nonuniformly rotating electrically conductive fluid. Journal of Physical Studies. **27**, 2403 (2023).

[24] Wolf A., Swift J. B., Swinney H. L., Vastano J. A. Determining Lyapunov exponents from a time series. Physica D: Nonlinear Phenomena. **16** (3), 285–317 (1985).

[25] Sandri M. Numerical Calculation of Lyapunov Exponents. The Mathematica Journal. **6** (3), 78–84 (1996).

[26] Cuomo K. M., Oppenheim A. V. Circuit implementation of synchronized chaos with applications to communications. Physical Review Letters. **71**, 65–68 (1993).

[27] Larsen R. W. LabVIEW for Engineers. Upper Saddle River, Prentice Hall/Pearson (2011).

[28] Kopp M., Kopp A. A New 6D Chaotic Generator: Computer Modelling and Circuit Design. International Journal of Engineering and Technology Innovation. **12** (4), 288–307 (2022).

[29] Kopp M., Kopp A. A New 8D Lorenz-like Hyperchaotic System: Computer Modelling, Circuit Design and Arduino Uno Board Implementation. Journal of Telecommunication, Electronic and Computer Engineering. **15** (2), 37–46 (2023).

[30] Lin H., Wang C., Yu F., Sun J., Du S., Deng Z., Deng Q. A. Review of Chaotic Systems Based On Memristive Hopfield Neural Networks. Mathematics. **11** (6), 1369 (2023).

[31] Deng Q., Wang C., Lin H. Memristive Hopfield neural network dynamics with heterogeneous activation functions and its application. Chaos, Solitons & Fractals. **178**, 114387 (2024).

Хаотична динаміка нового 7D-генератора на основі мемристора: комп'ютерне моделювання та схемотехніка

Копп М. Й.[1], Самуйлик І.[2,3]

[1] *Інститут монокристалів, Національна Академія Наук України, пр. Науки 60, 61072 Харків, Україна*
[2] *Інститут наук про життя та технології Даугавпілського університету, вул. Вієнібас 13, LV-5401, Даугавпілс, Латвія*
[3] *Інститут прикладної математики Ризького технічного університету, LV-1048 Рига, Латвія*

У цій статті представлена нова семивимірна (7D) хаотична система на основі мемристорного емулятора, спроектованого за допомогою функції гіперболічного тангенсу. Ця система побудована з шестивимірної (6D) динамічної системи рівнянь, що описує процес генерації магнітного поля і є альтернативою динамо-машині Рікітаке, що описує інверсію магнітного поля Землі та інших космічних об'єктів. У дослідженні аналізується стійкість точок рівноваги у новій динамічній системі. Спектр показників Ляпунова та вимірність Каплана–Йорка розраховані за фіксованих параметрів семивммірної динамічної системи. Наявність додатного показника Ляпунова демонструє хаотичну поведінку нової динамічної 7D системи, а дробова вимірність Каплана–Йорка вказує на фрактальну структуру дивних атракторів. На основі результатів, отриманих у моделях Matlab–Simulink та LabVIEW у середовищі Multisim реалізовано генератор хаотичних сигналів для 7D хаотичної мемристивної системи. Моделювання хаотичної поведінки у середовищі Multisim демонструє результати, аналогічні результатам моделювання у моделях Matlab–Simulink та LabVIEW.

Ключові слова: *динамічні системи на основі мемристорів; хаотична поведінка; комп'ютерне моделювання; схемотехнічна реалізація.*